OUKA
Osaka University Knowledge Archive

| | |
|---|---|
| Title | Role of the Anion Layer's Polarity in Organic Conductors β″ -(BEDT-TTF)_2XC_2H_4SO_3(X = Cl and Br) |
| Author(s) | Akutsu, Hiroki; Uruichi, Mikio; Imajo, Shusaku et al. |
| Citation | Journal of Physical Chemistry C. 2022, 126(38), p. 16529-16538 |
| Version Type | AM |
| URL | https://hdl.handle.net/11094/89425 |
| rights | This document is the Accepted Manuscript version of a Published Work that appeared in final form in The Journal of Physical Chemistry C, © American Chemical Society after peer review and technical editing by the publisher. To access the final edited and published work see https://doi.org/10.1021/acs.jpcc.2c05126. |
| Note | |

*Osaka University Knowledge Archive : OUKA*

https://ir.library.osaka-u.ac.jp/

Osaka University

# Role of the anion layer's polarity in organic conductors β´´-(BEDT-TTF)$_2$XC$_2$H$_4$SO$_3$ (X = Cl and Br)

Hiroki Akutsu,[†,*] Mikio Uruichi,[‡] Shusaku Imajo,[§] Koichi Kindo,[§] Yasuhiro Nakazawa,[†] and Scott S. Turner[¶]

[†]Department of Chemistry, Graduate School of Science, Osaka University, 1-1, Machikaneyama, Toyonaka, Osaka 560-0043, Japan.

[‡]Institute for Molecular Science, Okazaki, Aichi 444-8585, Japan.

[§]Institute for Solid State Physics, The University of Tokyo, Kashiwa 277-8581, Japan.

[¶]Department of Chemistry, University of Surrey, Guildford, Surrey, GU2 7XH, U.K.

*Organic Conductors, Polar, Dope, BEDT-TTF, Band Structure, Fermi Surface*

**ABSTRACT:** A 2D organic conductor β´´-(BEDT-TTF)$_2$ClC$_2$H$_4$SO$_3$ (**1**) crystallized in the $P2_1/m$ and has a polar anion located on the mirror plane, parallel to the 2D BEDT-TTF conducting layer. A temperature-induced phase transition tilts the anion such that a component of its electric dipole becomes perpendicular to the conducting plane. This low temperature phase β´´-β´´-(BEDT-TTF)$_2$ClC$_2$H$_4$SO$_3$ (**1L**) has two crystallographically independent donor layers, A and B, each of which is bordered by the positive or negative side of the anion's dipole (←B→A←B→A←). This exposes each donor layer to different effective electric fields and leads to layers of A and B with dissimilar oxidation states. Consequently, the transition can be called temperature induced non-doped-to-doped transition. The low temperature phase (**1L**) is isomorphous with β´´-β´´-(BEDT-TTF)$_2$BrC$_2$H$_4$SO$_3$ (**2**) from room temperature to at least 100 K, suggesting that **2** is also doped and it shows a very broad MI transition at 70 K. Applying only 2 kbar of static pressure sharpens the MI transition, indicating that the tilted anion straightens and therefore we suggest that it can be termed a pressure-induced doped-to-non-doped transition.

## Introduction

Over the past five decades, molecular charge transfer (CT) salts have been developed, leading to the discovery of many conducting materials such as semiconductors, semimetals, metals, and superconductors.[1, 2] After the discovery of the BEDT-TTF-based paramagnetic superconductor, β´´-(BEDT-TTF)$_4$[(H$_3$O)Fe(C$_2$O$_4$)$_3$]·PhCN,[3] organic conductors incorporating magnetic moieties were attracted great interest.[4] In particular, the λ-BETS$_2$FeCl$_4$ family has unique electromagnetic properties that emerge from the interplay between magnetic (localized) and conducting (itinerant) electrons.[5]

During the past two decades, we have also prepared purely organic magnetic conductors consisting of donor molecules, such as TTF or BEDT-TTF, and organic magnetic anions.[6-11] Each anion combines a sulfo group (-SO$_3^-$) with an organic stable radical. We have also prepared magnetic conductors of M(dmit)$_2$ salts, where M = Ni, Pd, or Pt, with purely organic cationic aminoxyl radicals.[12, 13] The resulting salts have not yet shown any clear evidences of the interaction between the localized and itinerant electrons, although some have short contacts between S atoms of the donors and O and/or N of the spin center.[6, 8-9] The sulfonates also have relatively large dipole moments and we have noted that some of these polar ions provide CT salts with unique structural features, which we have classified into four types as shown in Figure 1. Almost all donor-anion type and acceptor-cation type salts consist of 1D or 2D conducting layers interleaved by insulating counterions with or without incorporated neutral molecules. Type I-IV salts have structurally unusual ionic layers, in which each individual polar ion aligns in the same orientation as the other ions in the same layer. The result is that each layer has a diploe moment.[6-13] In type I salts,[7-8, 10] the dipole moments of successive ionic layers oppose each other, as shown in Figure 1a, therefore there is no net dipole moment. However, type I salts have two crystallographically independent conducting layers (A and B) where one layer (A in Figure 1a) is bordered by the positive end of the dipole moment of the ionic layer and the other (B) is bordered by the negative end. We also observed self-doping in the type I salts, where the B layers were more positively charged than the A layers. By contrast, type III salts (Figure 1c)[12-13] provide no self-doping because the dipole moments of the ionic layers lie parallel to the conducting layers. Although Type III salts are similar to Type I, in that there is no net dipole moment. The self-doping effect of Type I salts has been reported by other groups. Tadashi Kawamoto, Takehiko Mori, et al. reported κ$_H$-(DMEDO-TSeF)$_2$[Au(CN)$_4$](THF), in which the electric dipole of tetrahydrofuran gives rise to interlayer charge disproportionation. This was confirmed by observing a difference in band fillings for the crystallographically independent two donor layers, as determined by Shubnikov–de Haas oscillations.[14] Tetsuo Kusamoto, Reizo Kato, et al. reported (Et-4BrT)[Ni(dmit)$_2$]$_2$ where Et-4BrT is ethyl-4-bromothiazolium,[15-16] which has a type I structure. The magnetic susceptibility and heat capacity measurements by Ryo Yoshimoto and Yasuhiro Nakazawa, et al. indicates that the salt is a Nagaoka ferromagnet, as a result of the partial hole doping of a Mott insulator. This means that electron-doped layers do not become ferromagnet. In fact it is clear that only one of the two crystallographically independent [Ni(dmit)$_2$]$_2$ layers becomes a ferromagnet.[17]

Thus far, type I, type II[9, 11] and type III salts have been provided from ions baring aminoxyl radicals from our group, but we have not yet reported any type IV salts. Reports of type I salts from other groups suggest that non-magnetic, smaller, and simpler anions can also provide polar anionic layers in organic conductors. Accordingly we have reported the BEDT-TTF, BEST, and BETS salts of the HOC$_2$H$_4$SO$_3^-$ anion[18] and the BEDT-TTF and BETS salts of BrC$_2$H$_4$SO$_3^-$.[19] In this article, we report a new BEDT-TTF salt of ClC$_2$H$_4$SO$_3^-$ and a new interpretation of the electronic structure of the previously reported BrC$_2$H$_4$SO$_3^-$ salt of BEDT-TTF.[19]

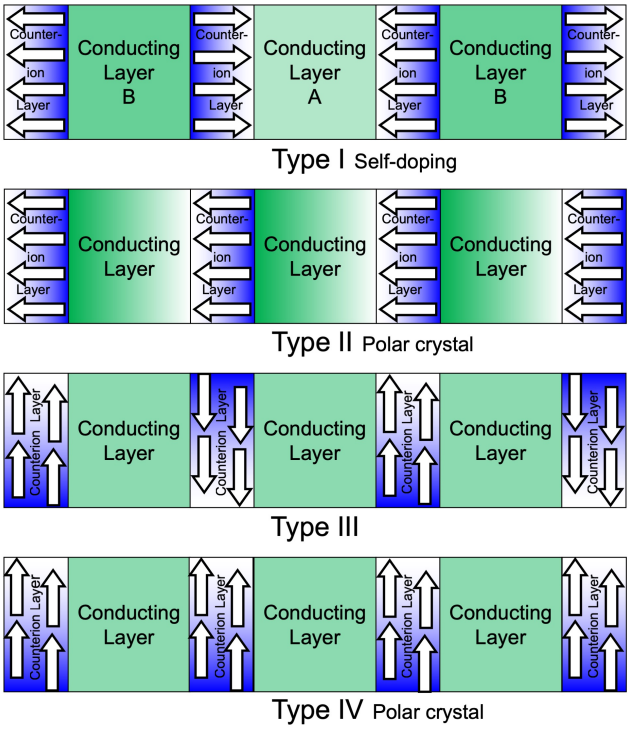


Figure 1. Schematic diagrams of the crystal structures of Type I-IV salts where the electrical dipoles of the counterions are indicated by arrows. Conducting layers are shown as green squares, and counterion layers are shown as blue rectangles.

## Methods

BEDT-TTF and $ClC_2H_4SO_3Na$ were purchased from Tokyo Chemical Industry and Chem-Impex International, Inc., respectively and used without further purification. Conventional constant current electrocrystallization (0.3 μA) at 10 °C in a mixed solvent of PhCl (18 mL) and EtOH (2 mL) with 10 mg of BEDT-TTF, 44 mg of $ClC_2H4SO_3Na$, and 67 mg of 18Crown6 ether in a H-shaped cells gave black needles. The X-ray diffraction measurements from 100 to 290 K were performed on a Rigaku XtaLAB Synergy Custom with MicroMax-007 HF/VariMax rotating-anode X-ray generator with confocal mono-chromated MoKα radiation. The crystal of **1L** is twinned consisting of two components 1 and 2, where the latter is rotated by 179.99° around the $c^*$-axis. A twin deconvolution with CrysAlis Pro (Rigaku 2015) and shelxl refinement[20] on olex2[21] gave the ratio of 1 and 2 of approximately 50: 50. Electrical resistivity measurements were performed by the conventional four-probe method using a HUSO HECS 994C1 four channel resistivity meter with cooling and heating rates of approximately 0.5 K/min. Magnetic susceptibility of a polycrystalline sample was measured from 2-300 K using a Quantum Design MPMS-2S SQUID magnetometer. The data were corrected for a contribution from the aluminum foil sample holder. The diamagnetic contribution of the sample was estimated from Pascal's constants. Dipole moments of the anions were calculated using MOPAC2016[22] with PM3 Hamiltonian on Winmostar V9.2.5, using the molecular geometries from the crystal structures with no further structure optimization. Effective voltages caused by the anion layers were estimated following Suda *et al.*[23] Band structures were calculated using a tight binding calculation package based on extended Hückel theory written by Prof. Takehiko Mori.[24-25] Raman spectra were measured on a Renishaw Ramascope, in Via Reflex. A diode laser (785 nm) was used to excite the sample, focused on an area of diameter ca. 5 μm, with ~0.1 mW power. The single crystal was fixed with silicon grease on a copper sample holder. The incident light was polarized to *c* and *b* axes for **1H** and **1L**, respectively. A low temperature spectrum was measured using a helium-flow cryostat Oxford MicrostatHe. Magnetoresistance measurements were performed in a $^4$He-cryostat with a non-destructive 60 T pulse magnet. The duration of the pulsed magnetic fields is about 36 ms.

## Results & discussion

Black needle-shaped crystals (**1**) were prepared by electrocrystallization. Variable temperature electrical resistivity of **1** is shown in Figure 2. Large resistivity jumps were observed at 210 K (cooling) and 260 K (heating), suggesting a drastic 1$^{st}$-class phase transition. Unfortunately, after the phase transition, almost all measured crystals became cracked. Therefore, figure 2 shows the resistivity curve of one of the measured twelve crystals. Several measured crystals show the resistivity jumps at the same temperatures as shown in figure S1. The room temperature conductivity of **1** is 6.5-190 S cm$^{-1}$. It is difficult to clearly state whether **1** is metallic or not from the curvature of the resistivity curve below the phase transition at 210 K. However, it is clear that the high temperature phase is metallic and the low temperature phase is not completely insulating because the highest resistivity value is less than twenty times larger than that at room temperature. This issue will be discussed in the final section.

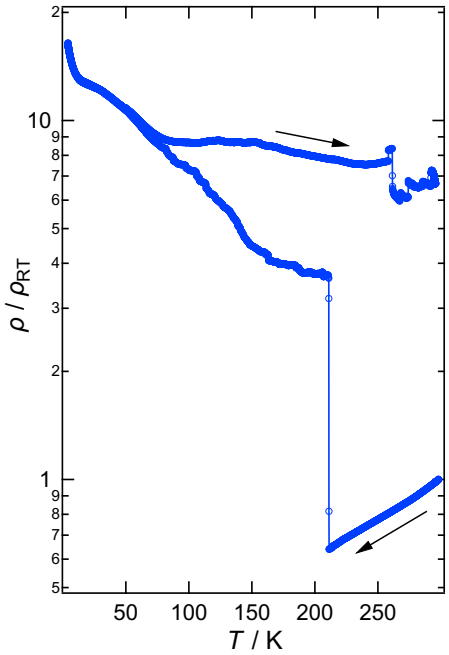


Figure 2. Temperature-dependent electrical resistivity of **1**.

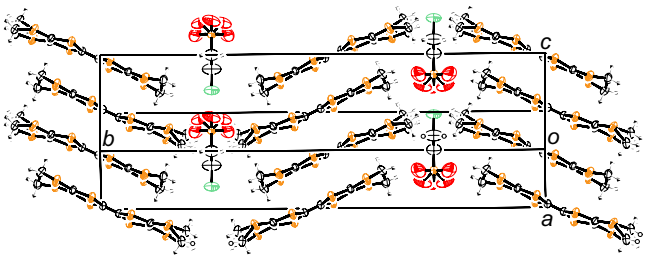


Figure 3. Crystal structure of **1H** at 290 K.

The crystal structure at 290 K, before cooling through the phase transition, gave the stoichiometry β′′-(BEDT-TTF)$_2$ClC$_2$H$_4$SO$_3$. The crystallographic data are shown in Table S1 and the crystal structure is shown in Figure 3. Hereafter we call the structure **1H** to indicate it is the high temperature phase. There is one BEDT-TTF and a half of anion in the asymmetric unit of **1H**. The salt crystallizes in the $P2_1/m$ space group with the anion located on the mirror plane with disorder of the oxygen atoms of the sulfo (-SO$_3^-$) group. The large and elongated thermal ellipsoids suggests that the sulfo group is rotationally disordered.

The salt crystallizes in a centrosymmetric space group, indicating no net dipole moment. The dipole moment of the anion, assuming no disorder is calculated using MOPAC2016[22] to be 5.7 debye. The anion is located on the mirror plane therefore the direction of the dipole's vector is plumb to the *b*-axis. Thus, **1H** is categorized as a type III structure (Figure 1). Thus far no special structural and/or electronic phenomena has been found in Type III salts.[12-13]

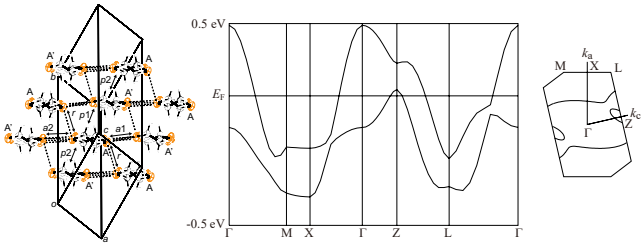


(a) (b) (c)

Figure 4. (a) A donor arrangement with intermolecular interactions, (b) band dispersions, and (c) Fermi surfaces of **1H**. Transfer integrals of *p*1, *p*2, *a*1, *a*2, and *r* are -1.86, -5.19, -9.01, -8.59, and -14.82 $\times 10^{-3}$, respectively.

Band structure calculations of the donor layer in **1H** were performed.[24-25] There are large electron Fermi surfaces and small hole pockets as shown in Figure 4, confirming that it is a stable metal, consistent with the resistivity behavior shown in Figure 2.

We have observed the phase transition by variable temperature X-ray analyses (Table S1). On cooling, the **1H** phase was present from 290 to 210 K and **1L** from 200 to 100 K. On heating **1L** persists from 100 to 250 K and then **1H** appears at 260 and 270 K. On cooling the crystal became twinned after the phase transition. In addition, crystals that were cooled below the phase transition temperature (210 K) and subsequently heated to above 260 K provided excellent reflections and low *R* values for **1H**, although the mosaicities are higher than for an uncooled sample. The crystal structure of **1L** is shown in Figure 5. The space group lowers to $P\bar{1}$ in **1L**. As noted above, **1L** is a twinned crystal, in which there are two components, component 2 (b) is rotated by 180° around the $c^*$-axis from component 2 (a), as shown in Figure 5. The asymmetric unit of **1L** has two crystallographically independent donors, forming two independent donor layers, and one anion. Thus, we indicate the donor layers by writing **1L** as β′′-β′′-(BEDT-TTF)$_2$ClC$_2$H$_4$SO$_3$. The sulfo group of the anion is ordered and not rotated, indicating that the order-disorder transition of the sulfo group occurs at the transition temperature. The anion is located on a general position. We used C=C and C-S bond lengths to estimate the charge on each BEDT-TTF molecule of **1L**,[26] although the *R* value of the X-ray analysis is not particularly low. The resultant charges for A and B are +0.57 and +0.55, respectively. The charges, normalized by the total number of holes in the asymmetric unit, are +0.51 and +0.49, respectively, suggesting the oxidation states of A and B donors are almost +0.5.

As shown in Figure 3, there is a V-shaped arrangement of adjacent donor columns in the *bc* plane of **1H.** By contrast, the donors in adjacent columns in **1L** are almost parallel. Thus donors of half of the layers located around $y = 0.0$ of **1H** turn one way and donors of the other layers located around $y = 0.5$ turn in the opposite direction during the phase transition. These movements are probably responsible for the single crystal of **1H** becoming a twinned crystal of **1L**. As mentioned above, if a crystal is cooled down to 100 K and subsequently heated up to room temperature, it provides a low *R* value, implying that the domain size of a single crystal region is small.

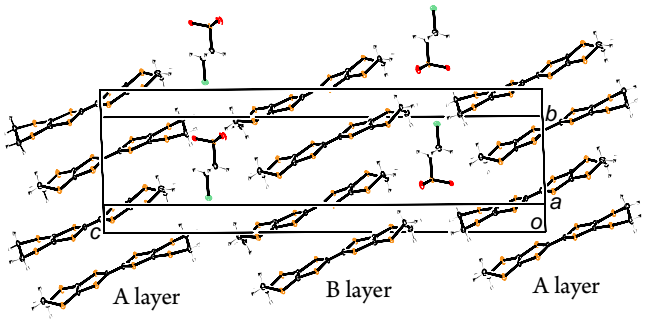


(a)

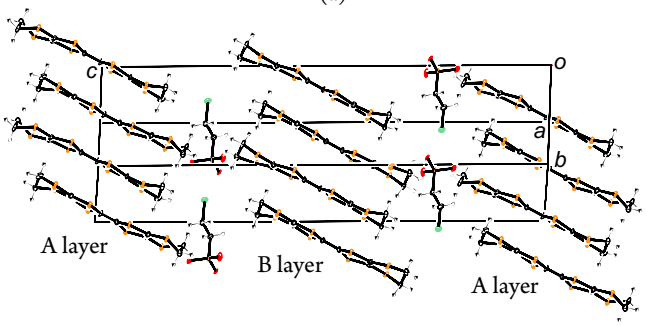


(b)

Figure 5. (a) Crystal structure of **1L** at 100 K, component 1, and (b) the structure rotated by 180° around the $c^*$-axis, component 2 in the twin crystal.

Band structure calculations of A and B layers were performed[24-25] as shown in Figure 6a and b, where both band fillings of 0.75 were used. The ratio of transfer integrals, $|p1 / p2|$ (if $|p1| > |p2|$ or $|p2 / p1|$ if $|p1| < |p2|$) are 1.24 and 2.44 for layers A and B, respectively, suggesting that the dimerization in layer B is stronger than that in layer A. The other values of both layers are quite similar and results in similar Fermi surfaces. The Fermi surfaces of **1L** are also like that of **1H**, the latter of which has slightly smaller hole pockets. The $|p2/p1|$ ratio for **1H** of 2.79 suggests that dimerization in **1H** is stronger when compared to layers A and B in **1L**.

Here we discuss the structural differences between **1H** and **1L**. The anion in **1H** is located on a special position, *m* (mirror), therefore the dipole's vector is exactly aligned in the same direction as the conduction plane. On the other hand, the anion in **1L** is located at a general position such that the direction of the dipole is slightly tilted from the 2D plane of the donor layer as schematically shown in Figure 7. The dipole moment of the anion in **1L** was calculated using MOPAC2016,[22] giving a value of 6.9 debye. The value is slightly larger than that in **1H** despite both molecules being the same. The disparity is caused by the difference of the geometries in each crystal

because no geometry optimization was applied in the MOPAC calculation, so that the atom positions obtained by each X-ray analysis were used. The anion in **1L** is tilted by approximately 9° from the conducting plane of the donor layer. This means that **1L** almost belongs to type III with some character of Type I. It is possible to estimate the effect of the tilt of the dipole moment on the nearest donor layer in terms of voltage using an equation as follows.[23]

$$\Delta\Phi = \frac{\mu N \cos\theta}{\varepsilon\varepsilon_0}$$

where $\Delta\Phi$ is an effective field in eV applied by the dipole moment, $N$ is the surface density of dipoles, $\mu$ is the effective dipole moment of the moiety, $\varepsilon_0$ is the permittivity of vacuum, $\varepsilon$ is the dielectric constant of the layer ($\approx 2$), and $\theta$ is the tilt angle of the moiety with respect to the conducting layer normal. The resultant value is 0.40 eV, meaning that the anion position applies an effective voltage of +0.40 V to donor layer A and -0.40 V to layer B. This suggests that layer B is more positively charged than layer A, namely interlayer charge disproportionation is expected. In addition, in **1L** there are two S···O contacts, shorter than the van der Waals distance (3.37 Å), between S atoms of BEDT-TTF and O atoms of -$SO_3^-$, at 3.024(8) and 2.956(8) Å for donor A and B, respectively. An asymmetry in the interactions between BEDT-TTF and -$SO_3^-$ often provides a charge disproportionation,[6,9,27] however in **1L** both interactions are similar, suggesting that the short S···O contacts are not compliant in this regard.

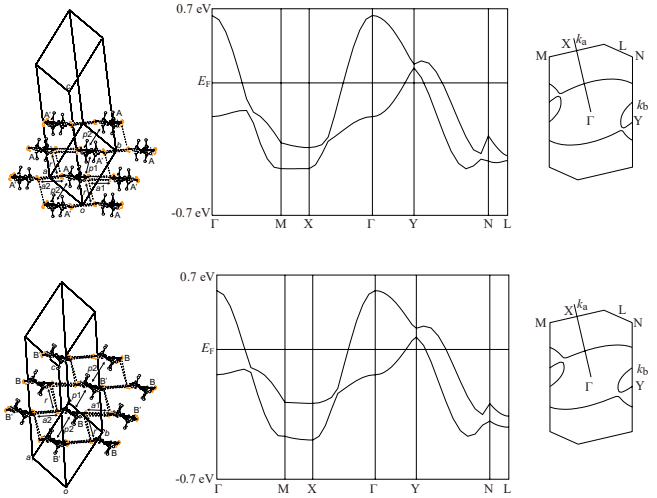


Figure 6. Donor arrangements (left), band dispersions (middle) and Fermi surfaces (right) of A layers (upper) and B layers (lower) of **1L**, where both band fillings are 0.75. Transfer integrals of $p1$, $p2$, $a1$, $a2$, and $r$ are -6.05, -7.51, -10.43, -10.24, and -15.59, respectively for A layer and -5.78, -2.37, -10.17, -10.53, and -15.25 × $10^{-3}$, respectively for B layer.

Here we try to estimation of the difference in charges between donors A and B caused by the 0.4 V effective voltage. Figure 8 shows the relationship between the difference of the formula charges between both independent donor layers and the effective voltage. At present, two metallic (orange circles)[7,14] and three semiconducting (pink circles)[8,10,17] type I salts have been reported, the parameters of which are plotted in Figure 9. Roughly, each set of metallic and semiconducting data points show linear tendencies, shown as orange and pink straight lines, respectively. The orange metallic line has a larger gradient than that of the pink semiconducting line. The $x$-intercept of the metallic line is zero but that of the semiconducting line is ≈ 1 V, suggesting that there is 1 V effective voltage threshold, below which no doping effects are observed. The black dashed line in Figure 8 indicates the effective voltage for **1L**, 0.40 V. The line crosses at approximately 0.02 for the difference in charges between cation layers. This value is too small to be confirmed using bond lengths determined by X-ray analysis (the error is ±0.1). Therefore, the doping level of **1L** should be confirmed using another method, which we will discuss in the final section. Since **1H** has no doping effect but **1L** does, the temperature-induced phase transition can be called "non-doped-to–doped transition". Now, we speculate on the mechanism of the transition. On cooling the rotation of the sulfo group stops, the anion tilts, the donor moves, and finally an electron hops from layer B to layer A.

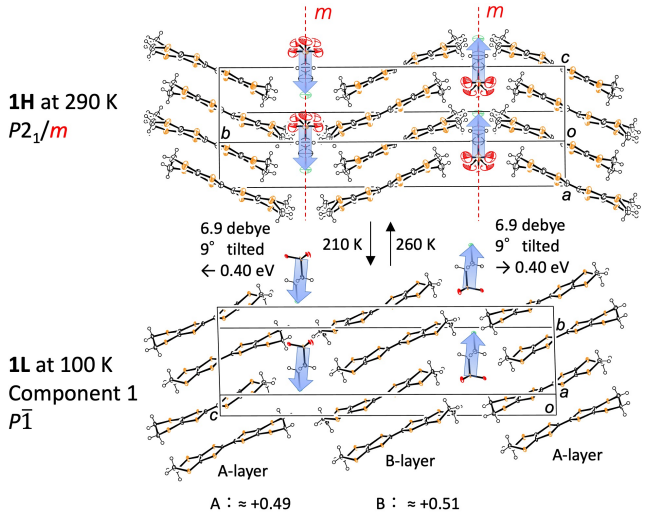


Figure 7. Comparison of the crystal structures of the high temperature (**1H**) and low temperature (**1L**) phases, where the arrow indicates the dipole moment of the anion.

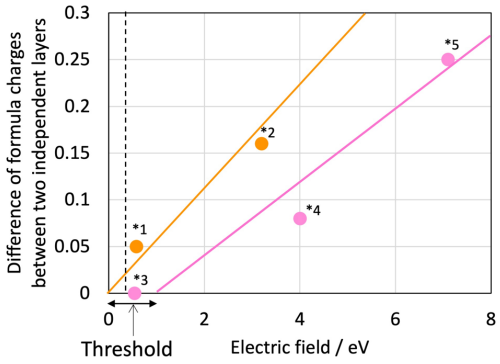


Figure 8. Relationship between effective electric field caused by the dipole moment of the anion layer and the difference of the charge between two independent donor layers in type I salts. Orange and pink circles indicate metallic and semiconducting salts, respectively.[28] The points were obtained from the salts, *1: $\kappa_H$-(DMEDO-TSeF)$_2$[Au(CN)$_4$](THF),[15] *2: κ-β′′-(BEDT-TTF)$_2$(PO-CONHC$_2$H$_4$SO$_3$) where PO is 2,2,5,5-tetramethyl-3-pyrrolin-1-oxyl,[7,9] *3: α′-α′-(BEDT-TTF)$_2$(PO-CONH-*m*-C$_6$H$_4$SO$_3$)·H$_2$O,[10] *4: (TTF)$_3$(PO-CON(CH$_3$)C$_2$H$_4$SO$_3$)$_2$,[8] and *5: the midpoint of (Et-2,5-DBrP)[Ni(dmit)$_2$]$_2$ and (Et-2I-5BrP)[Ni(dmit)$_2$]$_2$ where Et-2,5-DBrP is ethyl-2-iodo-5-bromopyridinium and Et-2I-5BrP is ethyl-2,5-dibromopyridinium.[17]

**1L** is isomorphous with β′′-β′′-(BEDT-TTF)$_2$BrC$_2$H$_4$SO$_3$ (**2**) from room temperature to at least 100 K. The crystal structure and

physical properties of **2** have already been reported.[19] **2** does not have a 1st-order phase transition but shows a broad MI transition at 70 K. In ref. 19, it was stated that **2** belongs to the type III category. However, in light of the discussion above, a more detailed analysis shows that the anion in **2** has a dipole moment of 9.9 debye[22] and is tilted by approximately 5.5° away from the conducting plane. The resultant effective voltage is 0.35 eV.[23] This suggests that salt **2** is in the interlayer charge disproportionate or doped state. However, the estimated molecular charges from bond lengths are +0.492 and +0.508 for A and B molecules, respectively, a small difference of only 0.016. The error in this empirical method[26] is approximately ±0.1 so this does not support doping in **2**. Nevertheless, there is evidence that **2** is doped. Ref. 19 and Figure 9 show the temperature dependences of the electrical resistivities under pressure for **2**. At ambient pressure (1 bar) there is a very broad MI transition at 70 K. The ratios of the resistivities of $\rho_{4.2\,K}$ and $\rho_{lowest}$ of only 24.7, 17.9 and 12.2 for samples 1,2, and in ref.19, respectively. The broad MI transitions imply that the doping effect makes the insulating ground state conductive. Moreover, applying only 2 kbar of pressure sharpens the MI transitions. The ratio of the resistivities of $\rho_{4.2\,K}$ and $\rho_{lowest}$ at 2 kbar are $9.00 \times 10^3$, $7.26 \times 10^2$, and $1.62 \times 10^4$ for samples 1, 2, and in ref.19, respectively. These are 365, 40.6, and 1330 times, respectively, larger than those at 1 bar. The MI transitions at 2 kbar seems to be typical for β′′-salts.[11,29-33] We speculate that applying the static pressure changes the tilt angle of the anions to almost zero, which induces a doped-to-non-doped transition. At first the anion straightens and the tilt angle becomes zero, then the donor may move (which will be confirmed in future work), and finally an electron jumps from layer A to layer B in order that both layers have the same band fillings. Namely compound **2** at 2 kbar is in the non-doped state, leading to a typical sharp MI transition.

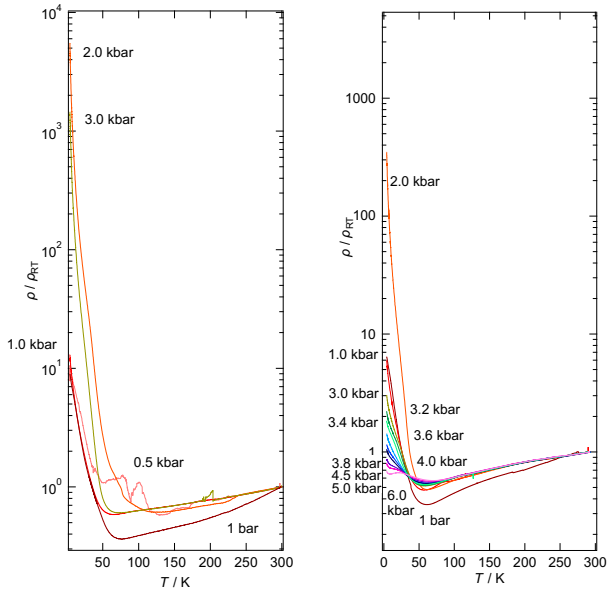


Figure 9. Temperature-dependent electrical resistivity under several static pressures of sample 1 (a) and 2 (b) of **2**.

The temperature-dependent magnetic susceptibility of **1** is shown in Figure 10. On cooling (red circles), there is an anomaly at 205 K, where the curve is bent. On heating (blue squares), an inflexion point is observed at 250 K. These anomalies appear to coincide with the structural phase transitions in **1**. The transition temperatures are slightly different from those observed from the resistivity curves, 210 and 260 K for the cooling and heating processes, respectively. The disparity may be caused by different rates of temperature change, 0.72 and 1.0 K/min for cooling and heating, respectively. On cooling, after the phase transition, the magnetic susceptibility decreases with decreasing temperature, which follows the same form as that of **2**[19] from room temperature to the MI transition temperature (70 K). Below 70 K the susceptibility of **2** decreases toward zero. By contrast **1** does not show zero susceptibility, suggesting that it does not show a MI transition. The magnetic susceptibility of **1** at the lowest temperature is ≈ $1.0 \times 10^{-4}$ emu mol$^{-1}$, which is relatively small when compared to Pauli paramagnetic metals of organic conductors (typically 2-6 × $10^{-4}$ emu mol$^{-1}$).[1] Moreover, Pauli paramagnetism is usually temperature-independent, so linear decrease is somewhat anomalous. Both salts have the same magnetic behaviors which are somewhat curious, suggesting that both electronic structures are quite similar.

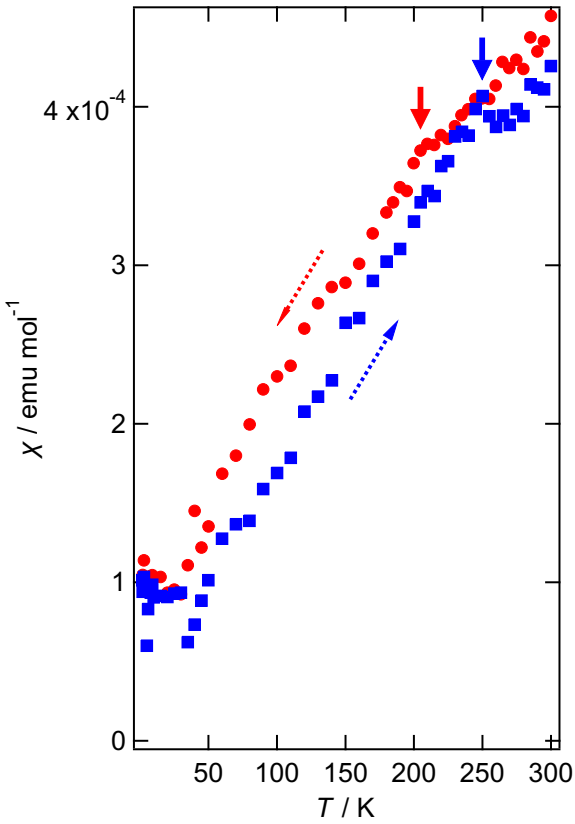


Figure 10. Temperature-dependent magnetic susceptibility per (BEDT-TTF)$_2$ClC$_2$H$_4$SO$_3$ of **1** after subtracting 0.074 and 0.081 % of $S = 1/2$ spins of Curie tails for cooling (red circles) and heating (blue squares) curves, respectively. The figure before the subtraction is shown in Figure S2. The directions of the temperature changes are shown by dotted arrows. The solid arrows indicate anomalies associated with the phase transition.

Finally, we tried to confirm the doping level of **1L** using several methods**.** Raman spectra of **1** and **2** were taken from 10-297 K (Figure S3). It is known that there is a linear relation between resonance $\nu_2$ and $Q$ (molecular charge of BEDT-TTF), where $\nu_2 = 1447 + 120(1 - Q)$.[34-35] Therefore, the $\nu_2$ peak would be expected to become a doublet on doping below the non-doped-to-doped transition temperature. However, only single peaks of $\nu_2$ at 10, 100, 240, and 297

K were observed. The width of the expected doublet can be calculated and is 2.4 $cm^{-1}$ for $Q_A$= 0.49 and $Q_B$ = 0.51. The width of 2.4 $cm^{-1}$ is shown by two vertical lines on each figure in Figure S2, suggesting that this difference would be too small to detect using the optical method. Moreover, the peak height reduces, and the peak broadens with increasing temperature, which is another barrier to determine $Q$ precisely. In addition, the spectra of **1** and **2** at all temperatures are quite similar to each other, indicating that both electronic structures are quite similar.

Temperature-dependent electrical resistivity of **1** under high magnetic field was determined. For the measurement 10 μmϕ of gold wires were used instead of 15 μmϕ used for the other resistivity measurements, which affords a better result from 1.4 to 200 K on heating as shown in Figure 11 together with that of **2**.[19] As previously mentioned, the MI transition of **2** is very broad, which is, we speculated, because of doping. Figure 11 indicates that the $\rho$ - log $T$ plots of both **1** and **2** are linear in the low temperature regions. The unusual temperature dependence was also observed in a charge-order-driven superconductor, β′′-(BEDT-TTF)$_4$[$(H_3O)Ga(C_2O_4)_3$]$PhNO_2$ ($T_c \approx 6$ K),[36] where the $\rho$ - log $T$ plots are linear from $T_c$ to 100 K. The authors addressed that this was caused by a weak localization with scattering centers introduced by the growth of small charge-ordered states. In our compound, the weak localization will be caused by significant doping of the strongly localized (perhaps charge-ordered) semiconducting phase.

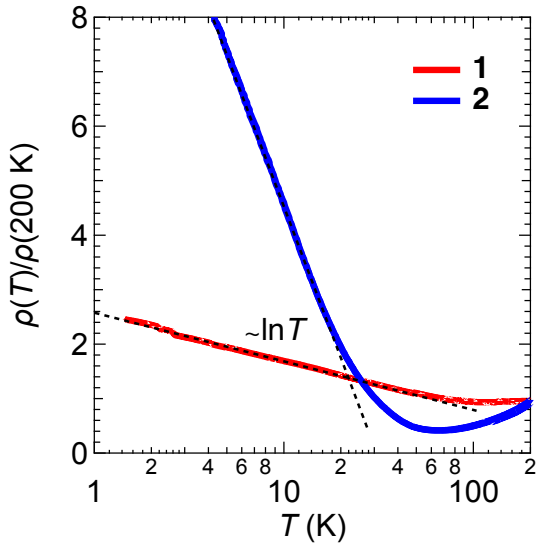


Figure 11. $\rho$ - log$T$ plots of **1** and **2**.

The Shubnikov-de Haas (SdH) effect is one of the most sensitive methods to detect differences in molecular charges.[7, 9, 14] According to our band structure calculations at 100 K, the estimated area of each Fermi surface of A and B layers, without doping ($Q_A = Q_B = 0.5$), of 3.9 (330) and 4.5 % (387 T) of the total Brillouin zone. With doping ($Q_A$ = 0.49, $Q_B$ = 0.51), each area of A and B layers are estimated to be 3.6 (302) and 5.0 % (420 T). The measurement results of **1** are shown in Figure 12. Figure 12c indicates that there is a Fermi surface with 106 T of amplitude, 1.3 % of area of the total Brillouin zone. The area is much smaller than estimated from band structure calculations of **1L**. A similar situation was observed in β′′-(BEDT-TTF)$_2$$AuBr_2$. Although Band structure calculations using X-ray data at room temperature provided only one hole pocket,[37,38] SdH experiments gave three frequencies. Several literatures[37-43] stated that this was due to Fermi surface nesting by a spin density wave (SDW), which occurred at 8 K at which a slight upturn with hysteresis in resistivity was observed. However, hysteresis was usually not occurred by SDW formation so that the upturn appeared to be caused by an antiferroelectric transition, similar to the transition of **1**. The calculated Fermi surfaces of β′′-(BEDT-TTF)$_2$$AuBr_2$ are similar to that of **1**, indicating that the similar nesting provides similar sharp and several Fermi surfaces. However, this is not the case that **1** provides only one and not so sharp fast Fourier transform (FFT) peak. We speculate that it is again indirect evidence of doping. The system becomes an insulator below 100 K, however the doping provides small hole and electron pockets, which were observed as an FFT signal. However, we were not able to determine the doping quantitatively from the SdH effect, but it will be qualitative evidence of the existence of doping. $^{13}$C NMR measurements using $^{13}$C-rich **1** may detect the difference.[44]

## Conclusions

The temperature or pressure induced tilt of a polar anion of less than ten degrees in two BEDT-TTF-based purely-organic conductors brings about a doping effect in the donor layer. These compounds are β′′-(BEDT-TTF)$_2$$XC_2H_4SO_3$ where X = Cl (**1**) and Br (**2**). **1** at room temperature (**1H**) is not doped, but shows a hysteresis in a temperature-induced non-doped-to-doped transition at 210 (cooling) and 260 K (heating). Salt **2**, shows a broad MI transition at 70 K, and it is isomorphous to **1L** with a tilted anion, suggesting that **2** is also doped. Applying only 2 kbar of static pressure sharpens the MI transition and it is suggested that this corresponds to straightening of the tilted anion. Hence **2** displays a pressure-induced doped-to-non-doped transition.

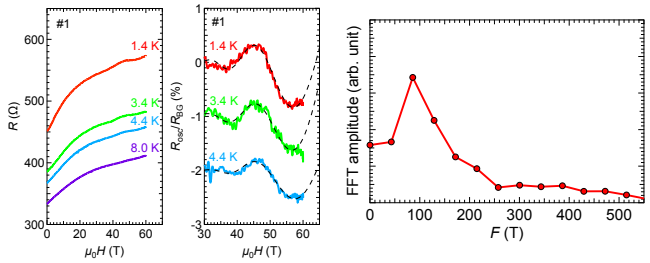


(a) (b) (c)

Figure 12. (a) $R(\Omega)$ - $\mu_0H$(T) and (b) $R_{OSC}$/ $R_{BG}$ (%) - $\mu_0H$(T) plots of magnetic field dependence of electrical resistivity and (c) fast Fourier transform (FFT) spectrum of Shubnikov-De Haas (SdH) oscillation of **1**.

## AUTHOR INFORMATION

### Corresponding Author

Hiroki Akutsu - Department of Chemistry, Graduate School of Science, Osaka University, 1-1, Machikaneyama, Toyonaka, Osaka 560-0043, Japan; https://orcid.org/0000-0002-8350-2246, Email: akutsu@chem.sci.osaka-u.ac.jp.

### Author Contributions

The manuscript was written through the contributions of all authors.

### Funding Sources

This work was partly supported by Scientific Research C (JP17K05751) from the Japan Society for the Promotion of Science (JSPS).

### Notes

The authors declare no competing financial interest.

## Supporting Information

The Supporting Information is available free of charge at https://*******. Temperature-dependent crystallographic data of **1**; Electrical resistivity of other three samples of **1**; Temperature-dependent magnetic susceptibility before subtracting Curie tails of **1**; Raman spectra of **1** and **2**

## ACKNOWLEDGMENT

A part of this work was conducted in Institute for Molecular Science, supported by Advanced Research Infrastructure for Materials and Nanotechnology (JPMXP1222MS1032) of the Ministry of Education, Culture, Sports, Science and Technology (MEXT), Japan.

## ABBREVIATIONS

TTF, tetrathiafulvalene; BEDT-TTF, bis(ethylenedithio)tetrathiafulvalene; dmit, 1,3-dithiol-2-thiole-4,5-dithiolate; CT, charge-transfer; MI, metal-insulator; BEST, bis(ethylenediseleno)tetrathiafulvalene; BETS, bis(ethylenedithio)tetraselenafulvalene.

## REFERENCES

(1) Williams, J.M.; Ferraro, J.R.; Thorn, R.J.; Carlson, K.D. ; Geiser, U.; Wang, H.H.; Kini, A.M.; Whangbo M.-H. *Organic Superconductor (Including Fullerenes) Synthesis, Structure, Properties and Theory*; Prentice-Hall, 1992.

(2) Mori, T. *Electronic Properties of Organic Conductors*; Springer Japan, 2016.

(3) M. Kurmoo, A. W. Graham, P. Day, S. J. Coles, M. B. Hursthouse, J. L. Caulfield, J. Singleton, F. L. Pratt, W. Hayes, L. Ducasse, et al. Superconducting and Semiconducting Magnetic Charge Transfer Salts: (BEDT-TTF)$_4$AFe(C$_2$O$_4$)$_3$.C$_6$H$_5$CN (A = H$_2$O, K, NH$_4$). *J. Am. Chem. Soc.*, **1995**, *117*, 12209-12217. DOI: 10.1021/ja00154a022

(5) Day, P.; Coronado, E. Magnetic molecular conductors. *Chem. Rev.* **2004**, *104*, 5419-5448. DOI**:** 10.1021/cr030641n

(5) Kobayashi, H.; Cui, H.; Kobayashi, A. Organic metals and superconductors based on BETS (BETS = bis(ethylenedithio)tetraselenafulvalene. *Chem. Rev.* **2004**, *104*, 5265-5288. DOI**:** 10.1021/cr030657d

(6) Akutsu, H.; Yamada, J.; Nakatsuji, S.; Turner, S. S. A novel BEDT-TTF-based purely organic magnetic conductor, α-(BEDT-TTF)$_2$(TEMPO-N(CH$_3$)COCH$_2$SO$_3$) · 3H$_2$O. *Solid State Commun.* **2006**, *140*, 256-260. DOI: 10.1016/j.ssc.2006.07.034.

(7) Akutsu, H.; Yamashita, S.; Yamada, J.; Nakatsuji, S.; Hosokoshi, Y.; Turner, S. S. A Purely Organic Paramagnetic Metal, κ-β″-(BEDT-TTF)$_2$(PO-CONHC$_2$H$_4$SO$_3$), Where PO = 2,2,5,5-Tetramethyl-3-pyrrolin-1-oxyl Free Radical. *Chem. Mater.* **2011**, *23*, 762-764, DOI: 10.1021/cm100984z.

(8) Akutsu, H.; Kawamura, A.; Yamada, J.; Nakatsuji, S.; Turner, S. S. Anion polarity-induced dual oxidation states in a dual-layered purely organic paramagnetic charge-transfer salt, (TTF)$_3$(PO-CON(CH$_3$)C$_2$H$_4$SO$_3$)$_2$, where PO = 2,2,5,5-tetramethyl-3-pyrrolin-1-oxyl free radical. *CrystEngComm* **2011**, *13*, 5281-5284. DOI: 10.1039/C1CE05578J.

(9) Akutsu, H.; Ishihara, K.; Yamada, J.; Nakatsuji, S.; Turner, S. S.; Nakazawa, Y. A strongly polarized organic conductor. *CrystEngComm* **2016**, *18*, 8151-8154. DOI: 10.1039/C6CE01865C.

(10) Akutsu, H.; Ishihara, Ito, S.; Nishiyama, F.; K.; Yamada, J.; Nakatsuji, S.; Turner, S. S.; Nakazawa, Y. Anion Polarity-Induced Self-doping in Purely Organic Paramagnetic Conductor, α′-α′-(BEDT-TTF)$_2$(PO-CONH-*m*-C$_6$H$_4$SO$_3$)·H$_2$O where BEDT-TTF is Bis(ethylenedithio)tetrathiafulvalene and PO is 2,2,5,5-Tetramethyl-3-pyrrolin-1-oxyl Free Radical, *Polyhedron* **2017**, *136*, 23-29. DOI: 10.1016/j.poly.2017.02.001.

(11) Akutsu, H.; Kohno, A.; Turner, S. S.; Yamashita, S.; Nakazawa, Y. Different electronic states of isomorphous chiral vs. racemic organic conducting salts, β′′-(BEDT-TTF)$_2$(*S*- and *rac*-PROXYL-CONHCH$_2$SO$_3$), **2020,** *1*, 3171-3175. DOI: 10.1039/d0ma00694g.

(12) Akutsu, H.; Turner, S. S.; Nakazawa, Y. New Dmit-Based Organic Magnetic Conductors (PO-CONH-C$_2$H$_4$N(CH$_3$)$_3$)[*M*(dmit)$_2$]$_2$ (*M* = Ni, Pd) Including an Organic Cation Derived from a 2,2,5,5-Tetramethyl-3-pyrrolin-1-oxyl (PO) Radical. *Magnetochem.* **2017**, *3*, 11. DOI: 10.3390/magnetochemistry3010011.

(13) Akutsu, H.; Ito, S.; Kadoya, T.; Yamada, J.; Nakatsuji, S.; Turner, S. S.; Nakazawa, Y. A new Ni(dmit)$_2$-based organic magnetic charge-transfer salt, (*m*-PO-CONH-*N*-methylpyridinium)[Ni(dmit)$_2$]·CH$_3$CN, *Inorg. Chim. Acta* **2018**, *482*, 654-658. DOI: 10.1016/j.ica.2018.07.003.

(14) Kawamoto, T.; Mori, T.; Graf, D.; Brooks, J. S.; Takahide, Y.; Uji, S.; Shirahata, T.; Imakubo, T. Interlayer Charge Disproportionation in the Layered Organic Superconductor κ$_H$-(DMEDO-TSeF)$_2$[Au(CN)$_4$](THF) with Polar Dielectric Insulating Layers. *Phys. Rev. Lett.* **2012**, *109*, 147005. DOI: 10.1103/PhysRevLett.109.147005.

(15) Kusamoto, T.; Yamamoto, H. M.; Tajima, N.; Oshima, Y.; Yamashita, S.; Kato, R. Bilayer Mott System Based on Ni(dmit)$_2$ (dmit = 1,3-dithiole-2-thione-4,5-dithiolate) Anion Radicals: Two Isostructural Salts Exhibit Contrasting Magnetic Behavior. *Inorg. Chem.* **2012**, *51*, 11645-11654. DOI: 10.1021/ic301552z.

(16) Kusamoto, T.; Yamamoto, H. M.; Tajima, N.; Oshima, Y.; Yamashita, S.; Kato, R. Bilayer Mott System with Cation···Anion Supramolecular Interactions Based on a Nickel Dithiolene Anion Radical: Coexistence of Ferro- and Antiferromagnetic Anion Layers and Large Negative Magnetoresistance. *Inorg. Chem.* **2013**, *52*, 4759-4761. DOI: 10.1021/ic400285a.

(17) Yoshimoto, R.; Yamashita, S.; Akutsu, H.; Nakazawa, Y.; Kusamoto, T.; Oshima, Y.; Nakano, T.; Yamamoto, H. M.; Kato, R. Electric dipole induced bulk ferromagnetism in dimer Mott molecular compounds. *Sci. Rep.* **2021**, *11*, 1332. DOI:

(18) Akutsu, H.; Koyama, Y.; Turner, S. S.; Furuta, K.; Nakazawa, Y. Structures and Properties of New Organic Conductors: BEDT-TTF, BEST and BETS Salts of the HOC$_2$H$_4$SO$_3^-$ Anion. *Crystals* **2020**, *10*, 775. DOI: 10.3390/cryst10090775.

(19) Akutsu, H.; Koyama, Y.; Turner, S. S.; Nakazawa, Y. Structures and Properties of New Organic Molecule-Based Metals, (D)$_2$BrC$_2$H$_4$SO$_3$ [D = BEDT-TTF and BETS]. *Magnetochem.* **2021**, *7*, 91. DOI: 10.3390/magnetochemistry7070091.

(20) Sheldrick, G. M. Crystal structure refinement with SHELXL. *Acta Cryst.* **2015**, *C71*, 3-8. DOI: 10.1107/S2053229614024218.

(21) Dolomanov, O. V.; Bourhis, L. J.; Gildea, R. J.; Howard, J. A. K.; Puschmann, H. OLEX2: a complete structure solution, refinement and analysis program. *J. Appl. Cryst.* **2009**, *42*, 339–341. DOI: 10.1107/S0021889808042726.

(22) Stewart, J. J. P. Stewart Computational Chemistry, Colorado Springs, CO, USA, http://OpenMOPAC.net. **2016**.

(23) Suda, M.; Kameyama, N.; Ikegaki, A.; Einaga, Y. Reversible Phototuning of the Large Anisotropic Magnetization at the Interface between a Self-Assembled Photochromic Monolayer and Gold. *J. Am. Chem. Soc.* **2009**, *131*, 865-870. DOI: 10.1021/ja808231c.

(24) Mori, T.; Kobayashi, A.; Sasaki, Y.; Kobayashi, H.; Saito, G.; Inokuchi, H. The Intermolecular Interaction of Tetrathiafulvalene and Bis(ethylenedithio)tetrathiafulvalene in Organic Metals. Calculation of Orbital Overlaps and Models of Energy-band Structures. *Bull. Chem. Soc. Jpn.* **1984**, *57*, 627-633. DOI: 10.1246/bcsj.57.627.

(25) Program Library of Energy Band Calculation for Molecular Conductors, Takehiko Mori, Tokyo Institute of Technology, Japan, http://www.op.titech.ac.jp/lab/mori/lib/program.html.

(26) Guionneau, P.; Kepert, C.J.; Bravic, G.; Chasseau, D.; Truter, R.M.; Kurmoo, M.; Day, P. Determine the charge distribution in BEDT-TTF salts. *Synth. Met.* **1997**, *86*, 1973-1974.

(27) Akutsu, H.; Yamada, J.; Nakatsuji, S.; Nakazawa, Y. A New BEDT-TTF-Based Organic Charge Transfer Salt with a New Anionic Strong Acceptor, *N*,*N*′-Disulfo-1,4-benzoquinonediimine. *Crystals* **2012**, *2*, 182-192. DOI: 10.3390/cryst2020182.

(28) Some effective voltages were calculated using our method. If the orange line is drawn only using the two experimental data points, the x-intersect becomes negative. This would mean that metals with zero effective electric

field have a different formula charge. Therefore, we tentatively include the origin as a third fixed point.
(29) Geiser, U.; Schlueter, J. A.; Dudek, J. D.; Williams, J. M. Structure of Bis(ethylenedithio)tetrathiafulvalenium Dichlorocyanoselenate (2:1), (BEDT-TTF)2Cl2SeCN. *Mol. Cryst. Liq. Cryst.* **1996**, *284*, 203-210. DOI: 10.1080/10587259608037923.
(30) Geiser, U.; Wang, H. H.; Schlueter, J. A.; Williams, J. M.; Smart, J. L.; Cooper, A. C.; Kumar, K.; Caleca, M.; Dudek, J. D.; Carlson, K. D.; et al. Synthesis, Structure, and Properties of the Organic Conductor (BEDT-TTF)$_2$Br$_2$SeCN. *Inorg. Chem.* **1994**, *33*, 5101-5107. DOI: 10.1021/ic00100a040.
(31) Li, W.; Rose, E.; Tran, M. V.; Hübner, R.; Łapiński, A.; Świetlik, R.; Torunova, S. A., Zhilyaeva, E. I.; Lyubovskaya, R. N.; Dressel, M. The metal-insulator transition in the organic conductor β″-(BEDT-TTF)$_2$Hg(SCN)$_2$Cl. *J. Chem. Phys.*, **2017**, *147*, 064503. DOI: 10.1063/1.4997198.
(32) Ozawa, T.; Tamura, K.; Bando, Y.; Kawamoto, T.; Mori, T.; Terasaki, I. Giant nonlinear conductivity in an organic conductor with a sharp metal-insulator transition: β″-(BEDT-TTF)$_3$(HSO$_4$)$_2$. *Phys. Rev. B* **2009**, *80*, 155106. DOI: 10.1103/PhysRevB.80.155106.
(33) Furuta, K.; Akutsu, H.; Yamada, J.; Nakatsuji, S.; Turner, S. S. The first organic molecule-based metal containing ferrocene. *J. Mater. Chem.*, **2006**, *16*, 1504-1506. DOI: 10.1039/b601614f.
(34) Yamamoto, T.; Uruichi, M.; Yamamoto, K.; Yakushi, K.; Kawamoto, A.; Taniguchi, H. Charge-Sensitive Vibrational Modes in Bis(ethylenedithio)tetrathiafulvalene. *J. Phys. Chem. B*, **2005**, *109*, 15226-15235. DOI: 10.1021/jp050247o.
(35) Yamamoto, T.; Uruichi, M.; Yakushi, K.; Kawamoto, A. Charge ordering state of β′′-(ET)$_3$(HSO$_4$)$_2$ and β′′-(ET)$_3$(ClO$_4$)$_2$ by temperature-dependent infrared and Raman spectroscopy. *Phys. Rev. B*, **2006**, *73*, 125116. DOI: 10.1103/PhysRevB.73.125116.
(36) Imajo, S.; Akutsu, H.; Kurihara, R.; Yajima, T.; Kohama, Y.; Tokunaga, M.; Kindo, K; Nakazawa, Y. Anisotropic Fully Gapped Superconductivity Possibly Mediated by Charge Fluctuations in a Nondimeric Organic Complex. *Phys. Rev. Lett.*, **2020**, *125*, 177002. DOI: 10.1103/PhysRevLett.125.177002.
(37) Wosnitza, J. Fermi *Surfaces of Low-Dimensional Organic Metals and Superconductors*; Springer, 1996, p.114-117.
(38) Mori, T.; Sakai F.; Saito, G.; Inokuchi, H. Crystal and band structures of an organic conductor β′′-(BEDT-TTF)$_2$AuBr$_2$. *Chem. Lett.*, **1986**, *15*, 1037-1040. DOI: 10.1246/cl.1986.1037.
(39) Kajita, K.; Nishio, Y.; Moriyama, S.; Sasaki, W.; Kato, R.; Kobayashi, H.; Kobayashi, A. Transport properties of a newly synthesized organic conductor, β′′-(BEDT-TTF)$_2$AuBr$_2$. *Solid State Commun.*, **1986**, *60*, 811-815. DOI: 10.1016/0038-1098(86)90602-2.
(40) Kurmoo, M.; Talham, D. R.; Day, P.; Parker, I. D.; Friend, R. H.; Stringer, A. M.; Howard, J. A. K. Structure and properties of a new conducting organic charge-transfer salt β-(BEDT-TTF)$_2$AuBr$_2$. *Solid State Commun.*, **1987**, *61*, 459-464. DOI: 10.1016/0038-1098(87)90491-1.
(41) Doporto, M.; Singleton, J.; Pratt, F. L.; Caulfield, J.; Hayes, W.; Perenboom, J. A. A.; Deckers, I.; Pitsi, G.; Kurmoo, M.; Day, P. Magnetotransport and Fermi-surface topology of β′′-(BEDT-TTF)$_2$AuBr$_2$: The effects of spin-density-wave formation. *Phys. Rev. B*, **1994**, *49*, 3934. DOI: 10.1103/PhysRevB.49.3934.
(42) Uji, S.; Aoki, H.; Tokumoto, M.; Ugawa, A.; Yakushi, K. Fermi surface and magnetoresistance in β′′-(BEDT-TTF)$_2$AuBr$_2$. *Physica B*, **1994**,*194-196*, 1307-1308. DOI: 10.1016/0921-4526(94)90983-0.
(43) Doporto, M.; Caulfield, J.; Pratt, F. L.; Singleton, J.; Hill, S.; Hayes, W.; Perenboom, J. A. A.; Kurmoo, M.; Day, P. High field magnetotransport studies of β′′-(BEDT-TTF)$_2$AuBr$_2$. *Synth. Met.*, **1993**, *56*, 2572-2577. DOI: 10.1016/0379-6779(93)90460-E.
(44) Ihara, Y.; Jeong, M.; Mayaffre, H.; Berthier, C.; Horvatić, M.; Seki, H.; Kawamoto, $^{13}$C NMR study of the charge-ordered state near the superconducting transition in the organic superconductor β′′-(BEDT-TTF)$_4$[(H$_3$O)Ga(C$_2$O$_4$)$_3$]·C$_6$H$_5$NO$_2$. *Phys. Rev. B*, **2014**, *90*, 121106. DOI: 10.1103/PhysRevB.90.121106.

## TOC Graphic